RSC Publishing PCCP

Structure and local reactivity of PdAg/Pd(111) surface alloys

Journal:	*Physical Chemistry Chemical Physics*
Manuscript ID:	CP-ART-08-2012-042914.R2
Article Type:	Paper
Date Submitted by the Author:	n/a
Complete List of Authors:	Mancera, Luis; Universitat Ulm, Institute of Theoretical Chemisty Behm, R J; Univ. Ulm, Inst. of Surface Chemistry and Catalysis Gross, Axel; Universitat Ulm, Institute of Theoretical Chemisty
Note: The following files were submitted by the author for peer review, but cannot be converted to PDF. You must view these files (e.g. movies) online.	
COPdAg_2012_final.tex	

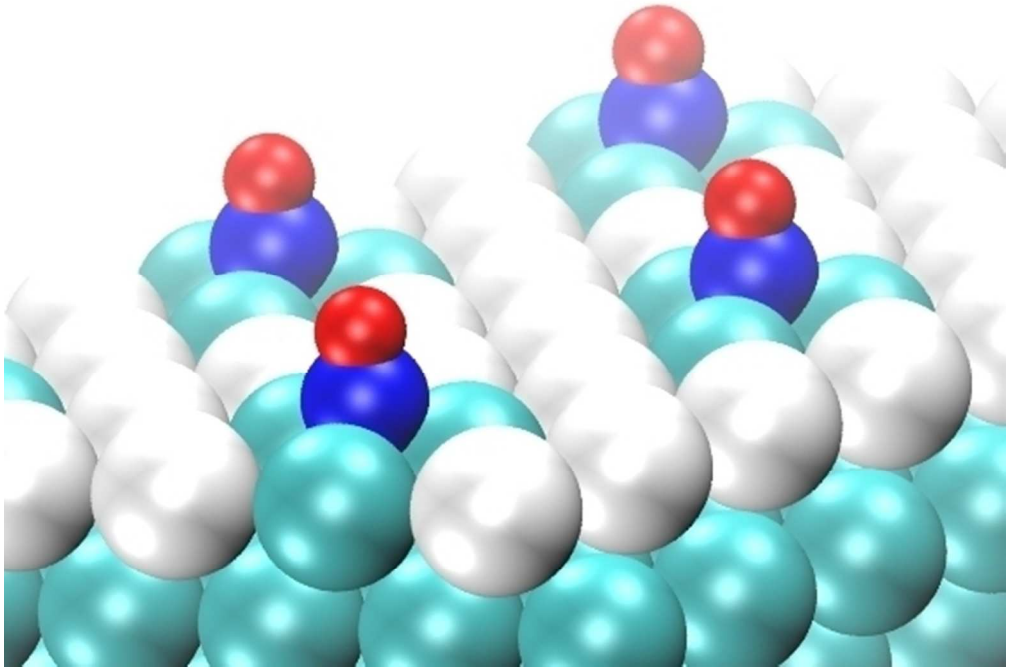

203x139mm (72 x 72 DPI)

Structure and local reactivity of PdAg/Pd(111) surface alloys

Luis A. Mancera,[1,*] R. Jürgen Behm,[2] and Axel Groß[1,†]

[1] *Institute of Theoretical Chemistry, University of Ulm, Albert-Einstein-Allee 11, D-89069 Ulm, Germany*

[2] *Institute of Surface Chemistry and Catalysis, University of Ulm, Albert-Einstein-Allee 47, D-89069 Ulm, Germany*

(Dated: November 22, 2012)

Motivated by a recent detailed experimental study [Y. Ma *et al.*, Phys. Chem. Chem. Phys. 13, 10741 (2011)], the structure and local reactivity of PdAg/Pd(111) surface alloys were studied using periodic density functional theory calculations. As a probe of the local reactivity, CO adsorption energies were evaluated as a function of concentration and configuration of silver and palladium atoms and the CO coverage and related to the underlying electronic structure. According to the calculations, the formation of PdAg/Pd(111) surface alloys is found to be energetically stable. We find in accordance with the experiment that the adsorption on the surface alloy is dominated by ensemble effects, whereas electronic ligand and strain effects effectively cancel each other. Furthermore, we elucidate the mechanism of CO adsorption on small Pd ensembles upon higher exposures.

I. INTRODUCTION

In the search for better catalyst materials in heterogeneous and electro-catalysis it has been noticed that catalysts composed by a combination of two metals offer different, and often higher, reactivity and selectivity than the pure components. [1–7] Different possible reactivity trends as a function of composition and concentration for a bimetallic surface can be obtained depending on the particular species forming the bimetallic system. For example, PdCu systems can show intermediate properties between those of the pure components as far as the interaction with adsorbates is concerned, [8–10] while for systems such as PtRu [11, 12] or PdAu [13–15] the adsorption properties are beyond those of the pure components.

In bimetallic catalysts, not only the size and shape of the metal nanoparticles are important parameters, but also the distribution of the two metals, which may depend sensitively also on their mixing ratio. The two components may either be more or less homogeneously distributed throughout the nanoparticle (bulk alloys), or a core of a specific composition is covered by a shell of a different composition. [16, 17] As a limiting case, core or shell may only exist of a single component.

Often a non-linear variation of the reactivity and selectivity is observed upon changes in the relative composition and distribution of the metal species in a bimetallic structure which is a result of having various simultaneous competing effects being operative, namely electronic ligand, strain and ensemble effects. [3, 18–27] Ideally, through an understanding of these various effects [28] a desired reactivity and selectivity may be obtained by deliberately tuning the composition and distribution of the components.

Because of the largely unknown vertical and lateral distribution of the two components in the catalytically active nanoparticles, which hinders a systematic understanding of their chemical and catalytic surface properties, structurally well defined planar model systems have found increasing interest. [13, 15, 17, 29] Such model systems include, e.g., pseudomorphic overlayers of one metal atom species deposited on a substrate formed by the other metal atom species, surface alloys or bulk alloys. [30]

Bimetallic PdAg catalysts have been used for reactions such as the oxidative dimerization of methane to ethane [31] and hydrogen separation, [32] and as a selective hydrogenation catalyst. [33–35] Previous studies on PdAg systems have mainly focused on bulk alloys, [36–41] surfaces of bulk alloys (alloy surfaces), [42–44] and supported cluster alloys, [45–48] while previous studies on PdAg surface alloys [49, 50] usually lack of information about lateral distribution of the atoms at the surface. Coulthard and Sham [36] studied the charge redistribution in PdAg bulk alloys using $L_{3,2}$-edge x-ray adsorption near edge structures (XANES) and x-ray photoemission spectroscopy. They showed that, relative to the pure element, both Pd and Ag gain d and lose non-d (s and p) charge upon alloying. Wouda *et al.*, [42] using scanning tunneling microscopy STM, have studied oxygen adsorption and migration on the PdAg(111) alloy surface. They observed a high segregation of silver together with a lower concentration of palladium at the surface. Recently, Tenney *et al.*, using a combination of STM and various spectroscopy techniques, have studied the effect of CO adsorption on bimetallic Ni-Au [51] and Pt-Au [52] clusters deposited on titania. They found that Ni and Pt atoms can migrate, in each case, from the bottom to the cluster surface in the presence of CO.

In spite of the various studies on PdAg catalysts, there is still a lack of studies of PdAg surface alloys, i.e. those systems in which the alloy occurs at the topmost layer. Here we report results of a theoretical study on the energetics and chemical properties of

* luis.mancera@uni-ulm.de

† axel.gross@uni-ulm.de

bimetallic PdAg/Pd(111) surface alloys based on density functional theory (DFT) calculations, using adsorption of CO as a probe of the local reactivity, motivated by recent experimental studies by Ma *et al.* [53, 54] using temperature-programmed desorption (TPD), X-ray photoelectron spectroscopy (XPS) and high-resolution electron energy loss spectroscopy (HREELS). Furthermore, a detailed (STM) study revealed that on these surface alloys the Pd and Ag surface atoms are almost randomly distributed in the topmost bimetallic layer. [55] Concerning the interaction of CO with the surface, it was observed that i) CO adsorption is not possible on Ag sites of the surface alloys for temperatures above 120 K, that ii) CO binding strength decreases significantly with increasing Ag concentration, and that iii) trends in CO adsorption energies seem to be dominated by ensemble effects, i.e., CO will preferentially adsorb on atomic groups with a certain size. We note that the important role of ensemble effects has also been observed in the oxygen adsorption on PdAg surface alloys. [56]

The unfavorable CO adsorption on silver above 120 K could be rationalized with the noble nature of this metal. As far as the local reactivity of the Pd atoms is concerned, two competing effects are operative which have for example also been identified for CO adsorption on PdAu/Au(111) [28, 57] and PtAu/Au(111) [58, 59] surface alloys. Exchanging Pd by Ag atoms in a PdAg surface alloy induces compressive strain because of the larger size of the Ag atoms. This compressive strain leads to a downshift of the *d*-band resulting in a weaker interaction with adsorbates. [26, 60] On the other hand, exchanging Pd atoms by Ag atoms in a Pd surface layer or in a PdAg surface alloy also increases the number of noble Ag atoms interacting more weakly with the Pd atoms. This (lateral) ligand effect causes an upshift of the *d*-band and a stronger interaction with adsorbates. [14, 25]

Following the experimental approach [53, 54] we have studied CO adsorption on various PdAg/Pd(111) surface alloys. As in the experimental study, we use the adsorption energy of CO as a probe of the local reactivity. By relating the calculated adsorption energies to the underlying geometric and electronic structure, we try to rationalize the results. Since it has been observed that trends in CO adsorption on PdAg/Pd(111) are affected by the size of Pd ensembles in the surface alloy, a significant part of this study will focus on the analysis of this effect. Finally, in response to the experimental observation of modified CO adsorption energies on Pd surface atoms after deposition of larger amounts of Ag (≥ 1 monolayer), where population of subsurface sites by Ag is plausible, we also investigated PdAg surface alloys with 1 or 2 Ag layers underneath. The results of this study will not only be relevant for the understanding of reactions in heterogeneous catalysis, but also in electrocatalysis where bimetallic electrodes are often employed. [61–64]

The remaining paper is organized into four sections: In Sec. II, we describe the relevant computational details. In Sec. III, we present a study of the Ag/Pd(111) pseudomorphic overlayers and the PdAg/Pd(111) surface alloys. In Sec. IV we investigate the CO adsorption on the PdAg/Pd(111) surface alloys. Conclusions are presented in Sec. V.

II. COMPUTATIONAL DETAILS

Plane-wave DFT calculations have been performed using version 4.6 of the VASP code, [65] together with the Perdew-Burke-Ernzerhof (PBE) [66] and revised-PBE (RPBE) [67] exchange-correlation functionals. The ionic cores are represented by projector augmented wave (PAW) potentials [68] as constructed by Kresse and Joubert. [69, 70] The electronic one-particle wave functions are expanded in a plane-wave basis set up to a cutoff energy of 400 eV. This cutoff energy, that corresponds to the maximum cutoff for the four atomic species considered in this study, was set up manually in order to keep it constant for all calculations. This value is larger enough than the default values preset in the code for palladium and silver. Default cutoff energies are already expected to provide convergence better than 1 mRy ($\sim$13 meV) in eigenvalues for this kind of basis set. Spin polarization is not considered due to the non-spinpolarized nature of the system. Dipole moment correction is set up in order to account for effects derived of using asymmetric slabs. Scalar relativistic effects are already included from the parametrization at the basis set generation. Convergence criteria for the electronic self-consistency and the ionic relaxation are set up to 1×10^{-5} and 1×10^{-4}, respectively. An enough large set of k-points was chosen in dependence on the cell size, in order to guarantee convergence. The relation between number of k-points and unit cell size is kept constant for all cases.

First, the bulk energy (E_b) and bulk lattice parameter (d_b) were computed using a FCC unit cell and a $11 \times 11 \times 11$ Γ-centered k-point grid. Values obtained using PBE/PAW for the bulk lattice parameter are 3.95 Å and 4.17 Å for Pd and Ag, respectively. These are in close agreement with the experimental values of 3.8898 Å and 4.0862 Å. [71] This yields nearest-neighbor distances $d_s = \frac{\sqrt{2}}{2} d_b$ of 2.80 Å and 2.95 Å for Pd(111) and Ag(111), respectively, which in the following we denote as surface lattice parameters.

The bimetallic surfaces are represented by periodic slabs consisting of five monolayers. The vertical height of the three-dimensional unit cell has been set to an integer number of the surface lattice parameter, $7d_s$, which allows us to have a separation between slabs close to 10 Å in all cases. Geometry optimization of the various surface configurations has been carried out keeping the two bottom Pd(111) layers fixed at their corresponding bulk positions while the three upper layers are fully relaxed.

Preliminary performance tests were performed using asymmetric and symmetric slabs, in order to choose the most reliable and efficient method to model the surfaces. Asymmetric slabs with five to ten layers were used with

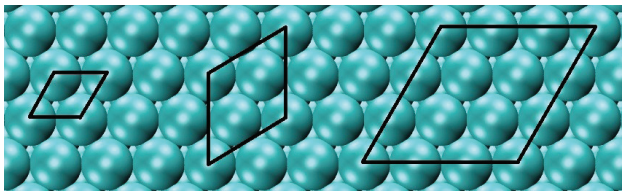

FIG. 1. Illustration of the unit cells used to represent the surface structures. **Left:** (1×1), **Center:** $(\sqrt{3} \times \sqrt{3})$R30°. **Right:** (3×3), mainly used to model the different Pd ensembles in PdAg/Pd(111) surface alloys.

relaxation of the three upper layers. Symmetric slabs with eight to ten layers were also investigated, relaxing the three external layers at each side of the slab. The vertical size of the unit cell has been chosen large enough in order to guarantee vacuum separation not smaller than 10 Å in all cases.

Three different surface unit cells (shown in Fig. 1) are used to represent the surfaces: (1×1), $(\sqrt{3} \times \sqrt{3})$R30° and (3×3). Surfaces are visualized using the Visual Molecular Dynamics (VMD) program. [72]

Geometry optimizations were performed using different Γ-centered k-point grids in dependence on the size of the unit cell in order to have equivalent geometry conditions, i.e., a $3 \times 3 \times 1$ k-point grid for the largest unit cell, a $5 \times 5 \times 1$ k-point grid for the intermediate one, and a $9 \times 9 \times 1$ k-point grid for the smallest one. For computing local density of states, a $9 \times 9 \times 1$ k-point grid was employed.

For the various structures studied here we use the following notation: Ag_{nL}/Pd(111) denotes a structure with n pseudomorphic silver overlayers above the Pd(111) substrate, PdAg/Pd(111) denotes a surface alloy at the topmost layer, and PdAg/Ag_{nL}/Pd(111) denotes a structure with a surface alloy at the topmost overlayer and n pseudomorphic silver layers underneath. In the case of a surface alloy, a certain number of silver atoms at the topmost pseudomorphic silver overlayer of a $\mathrm{Ag}_{(n+1)L}$/Pd(111) structure are replaced by palladium atoms.

Additional DFT calculations have been done using numbered atomic orbital (NAO) basis sets within the AIMS code, [73] and the PBE and RPBE exchange-correlation functionals. Using these basis sets allows for dealing with a larger vacuum between slabs, without significantly increasing the computing time. In this case, a unit cell height of $15d_s$ was used. The 'tight' settings built-in in the code for the basis sets were chosen. Same as for the VASP calculations, spin-polarization was not included and dipole correction was set up. Scalar relativistic effects were included through the atomic-zora method. [73] Convergence criteria for the electronic self-consistency is set up to 1×10^{-2} based on the sum of eigenvalues. Convergence criteria for the ionic relaxation is set up to 1×10^{-3}. Additional convergence criteria for total energy and charge density were set up to 1×10^{-5} and 1×10^{-4}, respectively. Other settings, including the k-point sets, were defined in an identical way than for the VASP calculations.

The main expected effect of using a larger vacuum level, which is one of the distinctive features of the NAO basis set in the AIMS code, should be a decrease of eventual large dipole moment effects. Nevertheless, this appears to do not be here so relevant, since such a dipole effect is already very small for this system. Since in addition the dipole correction is always set up in our calculations, the effect of using a larger vacuum in AIMS becomes less significant to this respect. Concerning accuracy, maximum differences in surface energy between both codes were of about 2 meV/Å^2, leading to similar trends in the overall values. Since results obtained with the NAO basis sets closely resemble those obtained using plane wave basis sets for the same functionals, as we will demonstrate for the surface energies of the pure Pd(111) and Ag(111) surfaces, we report for the remaining values only those results obtained using plane wave basis sets within the VASP code.

III. SILVER/PALLADIUM BIMETALLIC SURFACE ALLOYS

A. Pd(111) and Ag(111) surfaces

Surface energies (E_S) are evaluated as follows:

$$E_S = \frac{1}{2A}\left(E_{slab} - N_{\mathrm{Pd}}E_{\mathrm{Pd}_{bulk}} - N_{\mathrm{Ag}}E_{\mathrm{Ag}_{bulk}}\right), \quad (1)$$

where E_{slab} is the total energy for the slab (in eV) per unit cell. $E_{\mathrm{Pd}_{bulk}}$ and $E_{\mathrm{Ag}_{bulk}}$ are the palladium and silver bulk energies, respectively (in eV/atom). N_{Pd} and N_{Ag} denote the number of atoms of each species in the unit cell, and A is the area of the surface unit cell in Å^2. Surface energies reported throughout this study are mainly expressed in meV/Å^2 units. In order to convert these values into the also widely used J/m^2 units, the following conversion factor can be used: 1 meV/Å^2 $\sim$ 16.02×10^{-3} J/m^2 (conversely: 1 J/m^2 $\sim$ 62.42 meV/Å^2).

In order to check the optimum slab size, we performed test calculations using various asymmetric and symmetric slabs as described in Sec. II. Figure 2 shows surface energies for pure Pd(111) and Ag(111) surfaces at different slab sizes.

Ag(111) exhibits a faster convergence of the surface energy as a function of the number of layers than Pd(111). In addition, an odd-even oscillation is observed in the surface energy values for silver as a function of the number of layers. Using a symmetric slab leads to a reduction of the surface energy by $\sim$ 9 meV/Å^2 for palladium and by $\sim$ 6 meV/Å^2 for silver with respect to the asymmetric slab. This is simply a consequence of the relaxation of the other surface.

We note that similar trends in the surface energy as a function of slab thickness have also been reported by

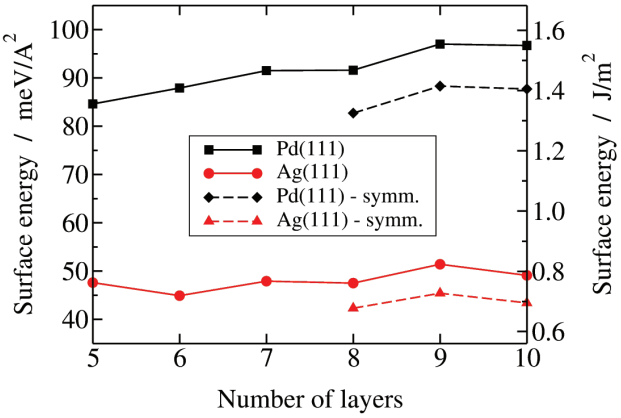

FIG. 2. Surface energies for Pd(111) and Ag(111). Left values are given in meV/Å^2 while right values are given in J/m^2. Asymmetric and symmetric slabs with different number of layers at the PBE/PAW level of theory. For asymmetric slabs three layers are relaxed at one side. For symmetric slabs three layers are relaxed at each side.

Singh-Miller and Marzari. [74] In the following, for the sake of the computational effort we have used a slab thickness of 5 layers for all considered bimetallic systems although for Pd(111) the surface energy is not converged at this number of layers. However, as we are mainly interested in trends in the local reactivity as a function of the composition of the surface alloys, five-layer slabs appear to be sufficient.

Table I shows the main results using the PBE and RPBE functionals with two different basis sets for the pure Pd(111) and Ag(111) surfaces, in comparison with theoretical results from other authors and with experimental results. PBE/PAW and PBE/NAO correspond to computations performed using the VASP and AIMS codes, respectively. Here five-layer asymmetric slabs were employed relaxing the three upper layers. It is worth to notice that for the PBE functional both type of basis sets used lead to rather similar results. The same occurs for the RPBE functional. Although the energy values calculated using RPBE are smaller that those using PBE, the trends in the values are similar independent of the choice of the basis set.

Note that we report surface energies for asymmetric slabs where the surface atoms have only been relaxed at one side of the slabs. These surface energies can not be directly compared to experimental values since they correspond to the mean value of the surface energies of the relaxed side of the slab and the unrelaxed side of the slab. Still, we report the computed energies together with experimental surface energy values reported by Mezey and Gibel, [79] in order to derive trends among the considered bimetallic structures. We obtained theoretical surface energies that are about 0.4 to 0.6 times the value of the corresponding experimental values extrapolated at T=0 (see Table I). Nevertheless, this large disagreement with the experimental values does not rely on the fact of using asymmetric slabs, since the use of symmetric slabs leads even to smaller surface energies than the asymmetric slabs (see Fig. 2), thus to a larger disagreement theory-experiment. Without overlooking possible shortcomings of the level of theory used in our study, it is prudent first to focus on the large uncertainty associated to this kind of experiments.

Experimental techniques available for determining surface free energies are not trivial and are in general inaccurate. They are based on measurements of surface tension of liquids corresponding to metals at melting temperature, and are applied on isotropic crystals or polycrystalline elements, thus not yielding information of a particular surface facet. [76, 79, 80] In addition, different models are used in order to derive values of the surface energies from the experimental data. Although, under certain assumptions, values of surface energies can be obtained for various crystal structures and facets at different temperatures, the different methodologies used might also contribute to the experimental uncertainty. For example, Mezey and Gibel, [79] report surface energies calculated from experimental data for an extensive list of elements at room and at melting temperature. The surface energy at $T = 0$ K can be obtained from these values using linear interpolation. They compute constants of

TABLE I. Surface energies for 5-layer asymmetric Pd(111) and Ag(111) slabs. The experimental values are extrapolated to different temperatures ($T_0/T_a/T_m$ for zero, room and melting temperature, respectively). All values are in meV/Å^2 and also in J/m^2 (in parenthesis).

	Pd(111)	Ag(111)
This study		
PBE/PAW	84.6 (1.36)	47.6 (0.76)
PBE/NAO	83.0 (1.33)	48.3 (0.77)
RPBE/PAW	71.0 (1.14)	35.6 (0.57)
RPBE/NAO	69.6 (1.12)	36.2 (0.58)
Other theoretical studies		
LDA/FP-LMTO[a]	102.4 (1.64)	75.5 (1.21)
LDA/FCD-LMTO[b]	119.8 (1.92)	73.0 (1.17)
LDA/FP-LAPW[c]	116.7 (1.87)	–
PBE/FP-LAPW[c]	83.0 (1.33)	–
PBE/USPP[d]	81.8 (1.31)	–
PBE/EMTO[e]	102.9 (1.65)	55.6 (0.89)
PBEsol/EMTO[e]	129.8 (2.08)	76.8 (1.23)
Experimental[f]		
$T_0/T_a/T_m$	135.7/127.5/85.9 (2.17/2.04/1.38)	85.9/81.3/65.3 (1.38/1.30/1.05)

[a] Reference 75.
[b] Reference 76.
[c] Reference 77.
[d] Reference 74.
[e] Reference 78.
[f] Reference 79.

proportionality to connect molar surface free enthalpies to surface free enthalpies, but depending on how these constants are averaged, these can lead to average errors from ∼7% up to ∼36%.

Various theoretical studies aimed at rationalize experimental surface energies have been carried out, mainly using first-principles methods (see values reported in Table I). Singh-Miller and Marzari [74] present a GGA-based DFT study with the PBE exchange-correlation functional and an ultrasoft pseudopotential (USSP) basis set, that gives very similar values for the surface energy we found for palladium. A similar value for palladium is also reported by Da Silva *et al.* [77] using PBE with the full-potential linearized augmented plane-wave (FP-LAPW) method. On the other hand, LDA-based DFT studies appear to have a better agreement with the experimental values of surface energies for low-index surfaces of 4*d* transition metals, even if the theory-experiment differences are still rather large. Such is the case of studies by Methfessel *et al.* [75] using the full-potential linear-muffin-tin-orbital (FP-LMTO) method, Vitos *et al.* [76] using the full charge density (FCD) LMTO method, or Da Silva *et al.* [77] using the FP-LAPW method. More recently, Ropo *et al.* [78] studied bulk and surface properties of 4*d* transition metals using the exact-muffin-tin-orbital (EMTO) method and various exchange-correlation functionals. It can be concluded, after averaging differences theory-experiment for various metals, that although PBEsol [81] functional provides results closer to the experiment for palladium, PBE still shows slightly overall better agreement with the experimental values than PBEsol. Due to the presumably inaccuracy of experimental data and the presumably best average performance of PBE to compute surface energies, we believe that this functional is well suited to describe the energetic trends in our study.

B. Ag/Pd(111) pseudomorphic overlayers

Next, we have computed surface energies for the pure monoatomic surfaces and for Ag_{nL}/Pd(111) surfaces with n silver pseudomorphic overlayers (n =1, 2, or 3) for asymmetric slabs. Note again that thus the surface energy corresponds to the mean value of a relaxed and a unrelaxed surface. However, in this way the surface energies can be compared to the energy cost of creating a Ag/Pd(111) interface. Additionally to the surface energies, we analyze the enthalpies of formation for the surfaces compared to a Pd(111) surface, i.e., the enthalpy change associated with the formation of a Ag_{nL}/Pd(111) bimetallic surface with respect to the clean Pd(111) surface and a silver bulk reservoir.

The enthalpies of formation (ΔH) are calculated according to Barabash *et al.* [82] as follows:

$$\Delta H = E_{\mathrm{Pd}_{(1-x)}\mathrm{Ag}_x/\mathrm{Pd}(111)} - E_{\mathrm{Pd}(111)} - x(E_{\mathrm{Ag}} - E_{\mathrm{Pd}}), \quad (2)$$

where $E_{\mathrm{Pd}_{(1-x)}\mathrm{Ag}_x/\mathrm{Pd}(111)}$ and $E_{\mathrm{Pd}(111)}$ are the total energy per surface atom of the $Pd_{(1-x)}Ag_x$/Pd(111) slab and the pure Pd(111) slab, respectively. E_{Ag} and E_{Pd} correspond to the bulk energy of silver and palladium, respectively. x denotes the relative amount of palladium atoms replaced by silver atoms at the surface. In this sense, the enthalpy of formation is the energy difference between the final PdAg/Pd(111) surface and the pure Pd(111) surface after replacing some palladium atoms by silver atoms from a bulk reservoir. [58]

Table II shows both sets of values calculated using PBE/PAW. Surface energies for the bimetallic surfaces have intermediate values between the pure silver and pure palladium surfaces as might be expected since they have both a Pd and a Ag termination. However, the relation is not linear.

Interpreting the results collected in Table II, it is first important to note that the surface energy of the pure Pd slab is higher than the surface energy of the pure Ag slab. This is a consequence of the higher cohesive energy of Pd which makes it more costly to cleave a Pd crystal. [75] The difference in surface energies between the Ag_{5L}/Pd_{0L} and the Ag_{5L} slab is just a consequence of the mismatch between the lattice parameters of the Pd(111) and Ag(111) surfaces of about 0.15 Å that induces a lateral contraction of the silver layers with the lateral Pd lattice constant by ∼ 5%.

The surface energy of the Ag_{1L}/Pd_{4L} pseudomorphic overlayer system of 63.6 meV/Å^2, however, is lower than the average between the pure Pd and Ag slab with the Pd lattice constant, and it is even lower than the surface energy for the pure Ag slab with the Pd lattice constant. This shows that the energy to create a Pd termination is overcompensated by the energy gain of creating a Ag/Pd interface indicating the presence of a relatively strong ligand effect between Ag and Pd. This attractive interaction is also reflected in the negative enthalpy

TABLE II. Surface energies (E_S) and enthalpies of formation (ΔH) for pure Pd(111) and Ag(111) surfaces and for Ag_{nL}/Pd(111) pseudomorphic overlayers, varying the number of silver layers. Surface energies in meV/Å^2 and enthalpies of formation in eV. Ag_{5L}/Pd_{0L} denotes the pure Ag(111) surface keeping the lateral lattice parameter of palladium whereas Ag_{5L} denotes the pure Ag(111) surface with the Ag lattice parameter. Note the conversion: 1 meV/Å^2 ∼ 16.02×10^{-3} J/m^2.

PBE/PAW		
	E_S	ΔH
Pd_{5L}	84.6	0.00
Ag_{1L}/Pd_{4L}	63.6	−0.28
Ag_{2L}/Pd_{3L}	70.7	−0.19
Ag_{3L}/Pd_{2L}	72.4	−0.17
Ag_{5L}/Pd_{0L}	66.4	−0.25
Ag_{5L}	47.6	−0.43

of formation of the Ag_{1L}/Pd_{4L} slab which demonstrates that the pseudomorphic overlayer is thermodynamically stable with respect to the formation of a pure Pd(111) surface and bulk Ag [2] in spite of the contraction of the Ag-Ag distance by $\sim 5\%$. Note, however, that every surface is under tensile strain since the lower coordination of surface atoms compared to bulk atoms leads to a stronger metal-metal binding. [60]

This coordination effect is no longer operative for second- and third-layer atoms. As a consequence, the surface energies increase and the formation enthalpies decrease for the Ag_{2L}/Pd_{3L} and Ag_{3L}/Pd_{2L} slabs compared to the Ag_{1L}/Pd_{4L} slab since the number of Ag atoms under compressive strain increases for a larger number of pseudomorphic Ag layers on Pd(111). Note that still the formation energy is negative indicating stability with respect to Ag segregation, however, it is strongly reduced compared to the case of just one Ag overlayer. These results are also consistent with experimental findings that show differences in the structure of a first and a second silver layer on Pd(111). Eisenhut *et al.*, [49] doing low-energy-electron-diffraction measurements, found that only one silver layer grows pseudomorphically on Pd(111) whereas a second silver layer already adopts a lattice constant close to the one of bulk Ag. It has been shown, however, in another study [83] that for Ag/Pt(111) this relaxation can be overcome by annealing.

Even if an enthalpy value can be calculated for the case of Ag_{5L} when the layers adopt the own lattice parameter for silver (see last entry in Table II), care has to be taken with this value since the lateral contraction effect due to palladium is not considered.

C. $Pd_{1-x}Ag_x$/Pd(111) surface alloys

Experimentally, a PdAg/Pd(111) surface alloy is created by depositing Ag atoms on Pd(111), and by subsequent annealing of the whole mixed surface. [50, 54] This results in a substitution of silver atoms at the topmost layer by palladium atoms. Even if the distribution of these substitute atoms is quite random for certain coverages, ensembles with different sizes can be differentiated using STM. [53, 55]

We have evaluated the surface energies and their relative stability for surface alloys with Pd_1, Pd_2, Pd_3, and Pd_4 ensembles at the topmost layer within a (3×3) geometry. An illustration of the considered ensembles is shown in Fig. 3 for the various PdAg/Pd(111) configurations: Pd_1Ag_8/Pd(111), Pd_2Ag_7/Pd(111), Pd_3Ag_6/Pd(111), and Pd_4Ag_5/Pd(111).

These configurations are the result of substituting 8, 7, 6, or 5 palladium atoms by silver atoms at the pure Pd(111) surface within the (3×3) unit cell. Or conversely, to the substitution of 1, 2, 3, or 4 silver atoms by palladium atoms at the pseudomorphic silver monolayer of the Ag/Pd(111) system represented with the same unit cell. We also have considered less compact Pd ensembles, but the minimum energy configurations were found to have the most compact structures, i.e. a triangle for Pd_3 and a rhombus for Pd_4. Since every particular ensemble is computed using the same (3×3) unit cell, the corresponding palladium coverage (θ_{Pd}) varies from 1/9 up to 4/9.

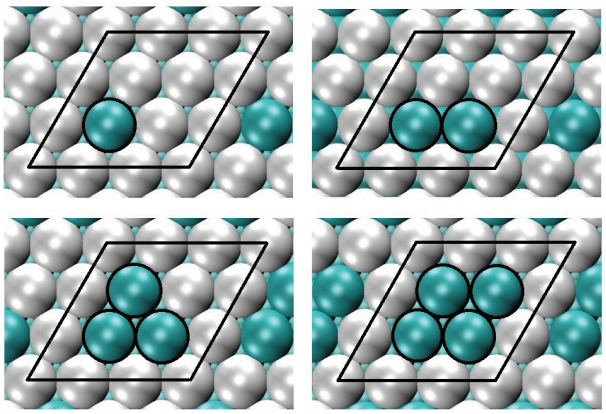

FIG. 3. Considered geometries for the PdAg/Pd(111) surface alloys, in which the alloy is at the topmost layer and all underneath layers are composed of palladium. The palladium ensembles correspond to groups of 1, 2, 3 or 4 atoms. (Pd: cyan, Ag: silver).

Results for the surface energies and enthalpies of formation are summarized in Table III. For the sake of completeness, we also include the results for PdAg surface alloys on Ag_{1L}/Pd_{3L} and Ag_{2L}/Pd_{2L} slabs in order to analyze the Pd-Ag interaction. For the first case in that table, the PdAg surface alloy on Pd(111), the surface energy increases steadily by increasing the Pd content and ensemble size. However, the increase is smaller for low contents (small ensembles) than for the larger Pd contents (larger Pd ensembles), indicating a non-zero ensemble size effect in the surface energy per Pd surface atom. A comparable behaviour is observed for the formation enthalpy, which decreases for a larger Pd contents. Note that experimentally an overall random distribution of the surface atoms is observed, with a slight tendency to cluster formation for low silver concentration (below 45%), a complete random distribution from 50% to 65%, and a slight preference for unlike nearest neighbors when the Ag concentration is above 75%. [53] The nearly linear relationship of the surface alloy enthalpy of formation with the substitution ratio for the $PdAg/Pd_{4L}$ structures is consistent with this experimental observation since it indicates that there is no significant preference for neither like nor unlike atom pairs in the surface alloy.

As already mentioned above, the replacement of a Pd termination by a Ag termination together with the favorable Pd-Ag interaction makes the Ag monolayer on Pd(111) to the most stable structure. Note that for $Pt_{(1-x)}Au_x$/Au(111) surface alloys, a qualitatively op-

posite trend in the surface alloy formation enthalpies has been observed [58, 59]: because of the larger cohesive energy of Pt than of Au, the PtAu surface alloy formation on Au(111) is energetically not stable with respect to the segregation of Pt bulk.

Interestingly enough, if a silver layer is added as the subsurface layer, the trends in the surface energies and enthalpies of formation are inverted. A second underlying silver layer, as in PdAg/Ag_{2L}/Pd_{2L}, however, leads to a more or less uniform surface energy and enthalpy values. To analyze these trends in more detail, the enthalpies of formation are plotted in Fig. 4 as a function of the Ag content in the uppermost layer, where also a lower silver content of 1/3 in a (3×3) unit cell has been included.

Comparing the stability of the PdAg/Ag_{1L}/Pd_{3L} surface alloys with those of the PdAg/Ag_{2L}/Pd_{2L} surface alloys, the differences are also easy to understand: The existence of an additional compressed Ag layer makes the PdAg/Ag_{2L}/Pd_{2L} surface alloys less stable than the corresponding PdAg/Ag_{1L}/Pd_{3L} surface alloys with respect to segregation into the pure metals. The most interesting finding, however, is the fact that for intermediate Ag concentration in the surface alloy the formation of the PdAg/Ag_{1L}/Pd_{3L} surface alloy is more favorable than the formation of the PdAg/Pd_{4L} surface alloy.

The experimental observation of a slight preference for unlike nearest neighbors for higher Ag concentration [53, 55] suggests an attractive Pd-Ag interaction, although these structures might not be in thermodynamical equilibrium but kinetically stabilized. Still this indicates that it might be more favorable for the PdAg surface alloys at low to intermediate Ag concentrations to be deposited on a Ag_{1L}/Pd_{3L} substrate. Hence, the existence of surface alloys in the near surface region can not be ruled out by these results even from purely energetic reasons and is again consistent with the experimental observation of interdiffusion between Ag film and Pd substrate at annealing temperatures above 500 K, [54] although under these conditions entropy effects are likely to be dominating. Note, however, that per Ag atom the formation of a Ag monolayer on Pd(111) is still more stable than the formation of a PdAg surface alloy on a Ag_{1L}/Pd_{3L} substrate.

TABLE III. Surface energies in meV/Å^2 (upper lines) and enthalpies of formation in eV (lower lines) for the considered PdAg/Ag_{nL}/Pd(111) surface alloys. 1 meV/Å^2 $\sim 16.02\times10^{-3}$ J/m^2.

PBE/PAW				
	Pd_1	Pd_2	Pd_3	Pd_4
θ_{Pd}	1/9	2/9	3/9	4/9
PdAg/Pd_{4L}	64.5	66.0	68.2	**70.5**
	−0.27	−0.25	−0.22	−0.19
PdAg/Ag_{1L}/Pd_{3L}	**69.7**	68.3	66.8	65.8
	−0.20	−0.22	−0.24	−0.26
PdAg/Ag_{2L}/Pd_{2L}	**71.8**	71.4	71.4	71.7
	−0.17	−0.18	−0.18	−0.18

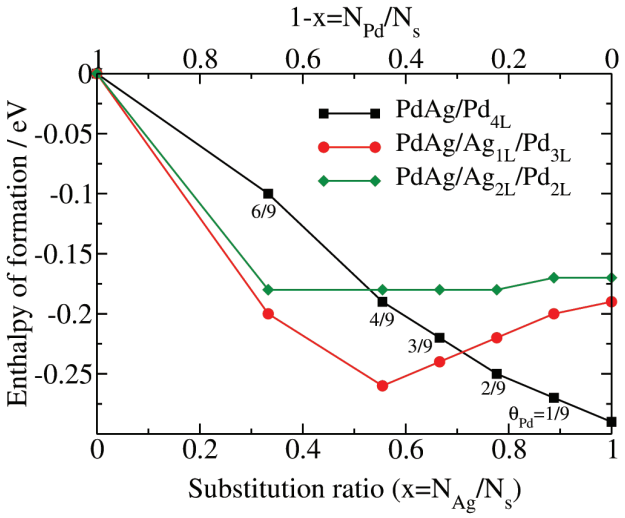

FIG. 4. Surface alloy enthalpies of formation ΔH, in eV, for the $Pd_{(1-x)}Ag_x$/Ag_{nL}/Pd(111) structures as a function of the substitution ratio x. The index nL denotes a certain number of silver layers between Pd(111) and the surface alloy. The substitution ratio x accounts for the number of palladium atoms replaced by silver atoms at the topmost layer. The upper horizontal scale for $1-x$ accounts for the relative number of palladium atoms at the topmost layer, that also corresponds to palladium coverage θ_{Pd} (labeled here at the first curve).

In order to predict the catalytic activity of the PdAg surface alloys as a function of their composition within the *d*-band model, [84, 85] we have determined the local density of states (LDOS) for Pd atoms in the topmost layer of three of the configurations shown in Fig. 3, i.e. Pd_1, Pd_2, and Pd_3 (palladium coverages are 1/9, 2/9 and 3/9 respectively). Figure 5 shows the local DOS projected onto the *d*-states for the pure Pd(111) surface and the three corresponding surface alloys. The center of the *d*-band for the pure Pd(111) surface is located at −1.53 eV. We observe that by alloying the band becomes narrower and consequently, [86] the center of the *d*-band shifts up slightly. In their study about charge redistribution in PdAg bulk alloys, Coulthard and Sham [36] show that, relative to the pure element, both Pd and Ag gain *d* and lose non-*d* (*s* and *p*) charge upon alloying. More precisely, that study suggests a depletion of *p* charge in Pd and a depletion of *s* charge in Ag, to compensate the gain of *d* charge in both elements. It is interesting that even at a large dilution of Pd on Ag, i.e. low composition of Pd and high composition of Ag, the Pd *d* orbitals would not be completely filled.

As mentioned above, alloying a transition metal with a noble metal of a larger size leads to two competing effects: compressive strain because of the addition of a larger atom vs. the weaker interaction of the transition metal

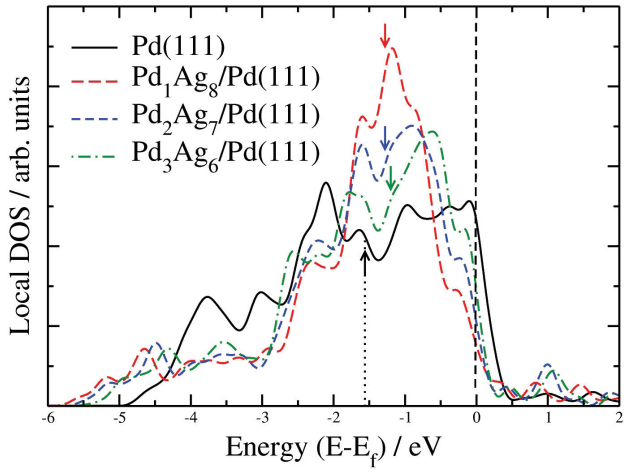

FIG. 5. Local density of d-states calculated by projection of the d wave functions onto the atomic orbitals at a palladium top-site. Four cases are represented: the pure Pd(111) surface and PdAg surface alloys containing Pd_1, Pd_2 and Pd_3 ensembles. All values are referred to the Fermi energy. Up-arrow denotes the position of the d-band center for the Pd(111) surface and down-arrows denote the position of the d-band center for the surface alloys.

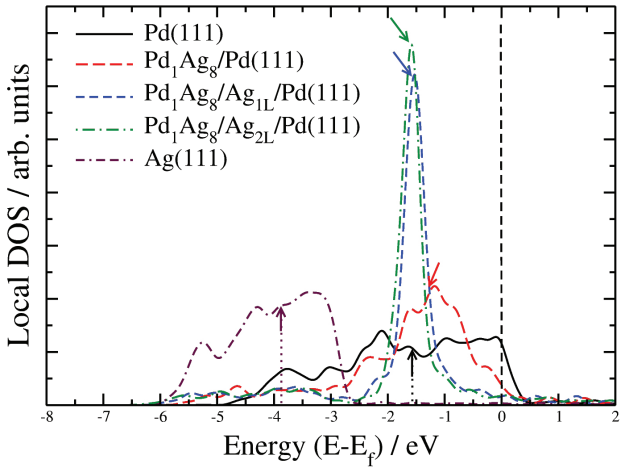

FIG. 6. Local density of d-states. Here we compare the pure Pd(111) and Ag(111) surfaces to the LDOS of the Pd atom of PdAg surface alloys containing only Pd_1 ensembles for different layer stacking in the first and second subsurface layers. Long up-arrows denote the center of the band of the pure surfaces, while short arrows denote the center of the band of the surface alloys.

atoms with the noble metal atom. [30] For PtAu/Au(111) surface alloys, both effects almost cancel. [58, 59]

Obviously, for PdAg/Pd(111) surface alloys with low Pd concentrations, the alloying with Ag leads in general to an upshift of the center of the d-band of the Pd atoms in the uppermost layer. For both the Pd_1 and Pd_2 ensembles, the center of the d-band shifts by about 0.2 eV to -1.34 eV, whereas for the Pd_3 ensemble the d-band center shifts further up to -1.30 eV. This suggests that the local reactivity of the Pd atoms in a PdAg/Pd(111) surface alloy is enhanced compared to the clean Pd(111) surface, which is due to the fact that the Pd atoms are embedded in a weakly interacting environment of noble Ag atoms. However, there is only a weak dependence on the number of Pd atoms for low Pd concentrations, indicating that ligand and strain effects cancel each other for Pd_1, Pd_2, and Pd_3 ensembles surrounded by Ag atoms.

In addition, we have also determined the LDOS of a Pd atom in a Pd_1Ag_8 surface alloy with Ag layers underneath the surface alloy (see Fig. 6). The LDOS of a Ag atom in a Ag(111) surface is also included. Replacing the Pd atoms in the subsurface layer by Ag leads to a strong narrowing of the LDOS at the Pd atom at the surface, which can be understood by the weaker coupling of the Pd atom to the Ag subsurface layer. Usually, such a narrowing of the band is associated with an up-shift of the local d-band for late transition metals because of charge conservation in the d-band. [26, 86] Note, however, that such an up-shift has also been found at Cu surfaces [87] although for the noble metal Cu the charge-conservation argument does not apply.

Interestingly enough, in this particular case in which the Pd atom is only surrounded by Ag atoms there is a slight unexpected down-shift of the local d-band of the Pd atom in the $Pd_1Ag_8/Ag_{1L}/Pd_{3L}$ and $Pd_1Ag_8/Ag_{2L}/Pd_{2L}$ surface alloys. Hence we expect a weaker binding of adsorbates to the Pd atom which is in fact in agreement with the experimental observation. [53] At the moment, we can only speculate about the reasons for this unexpected down-shift. Although the Pd-Ag interaction is weaker than the Pd-Pd interaction, it might still be strong enough – indicated by the negative enthalpy of formation of the Ag_{1L}/Pd_{4L} slab – to shift the Pd-LDOS towards the low-lying silver d-band.

IV. CO ADSORPTION ON SILVER/PALLADIUM BIMETALLIC SURFACES

A. The CO/Pd(111) system

Finally, we consider CO adsorption on the PdAg bimetallic surfaces in order to compare our results with the experiment. [53] but also as a local probe of the reactivity of the different sites in the bimetallic surfaces. Note that negative adsorption energies correspond to exothermic adsorption and that with binding energies the absolute value of the adsorption energies is meant. Note furthermore that in contrast to the experiment, CO adsorption energies can be calculated for all possible adsorption sites, not only for the stable ones.

First, we address the pure Pd(111) surface in order to evaluate the most favorable sites for CO adsorption and the trends in the CO adsorption energy as a function of coverage. This serves as a reference to analyze the

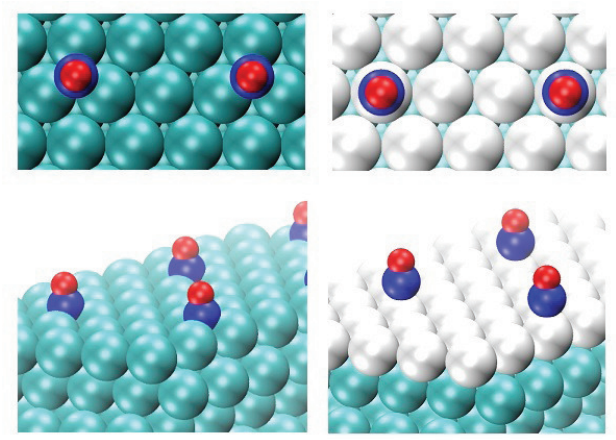

FIG. 7. Left panel: Adsorption of CO on hollow-fcc sites of the pure Pd(111) surface. Right panel: Adsorption of CO on top sites of a pseudomorphic silver overlayer above the Pd(111) substrate. Both cases correspond to a CO coverage $\theta_{CO} = 1/9$. (Pd: cyan, Ag: silver, C: blue, O: red).

changes in CO adsorption at the surface alloy systems. The left panel of Fig. 7 shows the most favorable configuration for CO adsorption on the pure Pd(111) surface at low CO coverages which corresponds to adsorption on fcc hollow sites.

Table IV shows the trends in the CO adsorption energies on pure Pd(111) as a function of the CO coverage. Here (3×3) and $(\sqrt{3} \times \sqrt{3})$R30° unit cells are used. We observe that CO adsorption on the pure Pd(111) surface preferentially occurs at the hollow sites, in agreement with experiment [88, 89] and previous theoretical studies, [25, 90] and it is stronger at the hollow-fcc site than at the hollow-hcp site for any of the considered CO coverages. Top-sites are less favorable for CO adsorption, with binding energies being ~ 0.5 eV higher than for the hollow sites. The larger the CO coverage, the lower the CO binding energy to the substrate. This can be rationalized by the increase of the mutual repulsion between the CO_{ad} molecules when these come closer to each other.

The good agreement theory-experiment for CO adsorption on the pure Pd(111) surface contrasts with the case of adsorption on a pure Pt(111) surface. In that case the experimental evidence of CO adsorption on a top site of Pt(111) does not match first-principle calculations predicting the fcc hollow site to be most stable. This problem has been widely discussed by Feibelman *et al.* [91] and in further studies by other authors. [92, 93] This discrepancy can be rationalized from the fact that first-principles calculations within the generalized gradient approximation considerably underestimate the energy gap between the highest occupied molecular orbital (HOMO) and the lowest unoccupied molecular orbital (LUMO) (See Ref. [58] and references therein).

Using RPBE/PAW leads to a CO binding to Pd(111) which is about ~ 0.3 eV weaker than using PBE/PAW. The RPBE values are also closer to the CO desorption energies from Pd(111) obtained in temperature programmed desorption experiments, [94] which yielded values of $\sim$1.2 eV for $\theta_{CO} = 1/3$ and $\sim$1.5 eV for $\theta_{CO} \leq 0.1$. Yet, all trends in the adsorption energies are unaffected by the choice of the functional. Since we are mainly interested in the structure-reactivity relationship for the PdAg bimetallic system, for which trends in adsorption energies matter, we will restrict ourselves to results obtained with the popular PBE functional.

TABLE IV. CO adsorption energies (in eV) calculated using PBE/PAW and RPBE/PAW for Pd(111) as a function of the CO coverage. The letters T, H, B denote top, hollow and bridge sites, respectively.

	PBE/PAW			RPBE/PAW		
θ_{CO}	1/9	1/3	2/3	1/9	1/3	2/3
T	−1.43	−1.38	−1.00	−1.17	−1.10	−0.68
H-fcc	**−2.06**	**−1.92**	**−1.46**	**−1.71**	**−1.58**	**−1.07**
H-hcp	−2.05	−1.91	−1.43	−1.70	−1.56	−1.04
B	−1.86	−1.75	−1.32	−1.53	−1.42	−0.95

B. The $CO/Ag_{nL}/Pd(111)$ pseudomorphic system

Next, we address CO adsorption on pseudomorphic Ag layers on Pd(111). The right panel of Fig. 7 illustrates the case of CO adsorption if the topmost overlayer is composed of silver atoms. The calculated adsorption energies for a low CO coverage of 1/9 at different adsorption sites are listed in Table V. In all cases, CO adsorption is weak, which is consistent with the experimental observation that CO adsorption on silver sites of PdAg/Pd(111) surface alloys occurs only for very low temperatures (below $\sim$ 120 K) [53, 54] at which CO diffusion to more favorable adsorption sites is frozen in. For one silver monolayer on Pd(111), CO adsorption, although weak, is most favorable at top sites. Additional silver layers do not modify the adsorption energies substantially, but in-

TABLE V. CO adsorption energies (in eV) calculated using PBE/PAW for pseudomorphic silver overlayers on the Pd(111) substrate, considering a fixed CO coverage of $\theta_{CO} = 1/9$. The letters T, H, B denote top, hollow and bridge sites, respectively

	PBE/PAW			
	Ag_{1L}/Pd_{4L}	Ag_{2L}/Pd_{3L}	Ag_{3L}/Pd_{2L}	Ag_{5L}
θ_{CO}	1/9			
T	**−0.14**	−0.14	**−0.15**	−0.20
H-fcc	−0.03	**−0.20**	−0.13	**−0.25**
H-hcp	−0.03	**−0.20**	−0.12	**−0.25**
B	−0.04	−0.17	−0.12	−0.23

terestingly enough, induce an alternation between most favorable adsorption at top- and hollow-sites for odd and even number of silver layers, respectively, which might be due to quantum size effects in the electronic distribution perpendicular to the surface as a function of the number of Ag layers.

Concerning CO adsorption on the pure Ag(111) surface, the calculated value (−0.25 eV) is in good agreement with the reported experimental chemisorption energy for this surface of -0.28 ± 0.02 eV. [95] This already weak CO chemisorption on a pure (111) silver surface is then further weakened by the effect of palladium sublayers as can be observed in Table V.

C. The CO/Pd$_{1-x}$Ag$_x$/Pd(111) system

Replacing Ag by Pd atoms in the topmost layer of Ag$_{1L}$/Pd(111) changes the strength of CO adsorption dramatically, as the CO adsorption energies listed in Table VI demonstrate. CO adsorption on a PdAg/Pd(111) surface alloy is energetically very favorable, particularly at the hollow-sites of palladium ensembles. Figure 8 shows an example of CO adsorption at the hollow-site of a triangular Pd$_3$ ensemble. The left panel represents the monolayer alloy, whereas the right panels exhibits a monolayer alloy with underlying silver layers.

In detail, Table VI shows the CO adsorption energies for different surface alloys and the effect of underlying silver layers. Since Pd$_3$ ensembles have only one hollow position, the study of CO adsorption in a (3×3) geometry imposed to set the Pd$_3$ ensembles either with a H-fcc site or with a H-hcp site, but not with both types of hollow sites in the same surface structure. This is not necessary for Pd$_4$ ensembles since they already have a H-fcc and a H-hcp site. Note that the Pd coverage is different in each particular case, since the same unit cell (3 × 3) is always used. If no underlying silver overlayers are present, the preferential adsorption sites are the hollow-fcc sites for Pd$_3$ and Pd$_4$ ensembles or, less stable the bridge sites for Pd$_2$. In fact, Pd$_3$ and Pd$_4$ show similar adsorption energies, what suggests that Pd$_3$ is the structure which determines the lowest adsorption energy and that the effect of additional surrounding Pd atoms is negligible. In this sense, experimental signals (TPD peaks, infrared bands) attributed to Pd$_3$ ensembles may originate not only from Pd$_3$ but also from larger ensembles. This ensemble effect is in agreement with experimental observations. [53] The CO adsorption energies at the top sites exhibit only a small variation as a function of the ensemble size, as also expected from the corresponding small shifts in the local *d*-band center plotted in Fig. 5. This is different from the ontop adsorption of CO on PdCu surface alloys, where ligand and strain effects do not cancel each other, but both lead to reduced CO adsorption energies at the top sites for higher Pd content in the surface alloys. [25] Experimentally, these shifts are not accessible, since CO would always adsorb on the more stable bridge or threefold hollow sites.

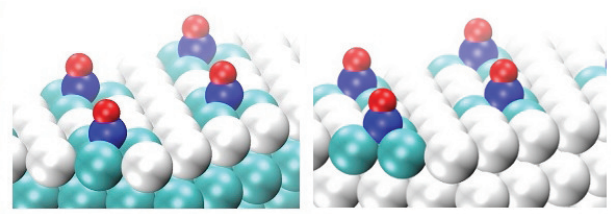

FIG. 8. Adsorption of CO on a hollow site of Pd$_3$ ensembles at the PdAg/Pd(111) surface alloy. **Left:** The pure monolayer alloy. **Right:** The topmost monolayer alloy with underlying silver layers. (Pd: cyan, Ag: silver, C: blue, O: red).

Note, however, that the CO binding energies on the Pd$_1$ monomer, the Pd$_2$ dimer and the Pd$_3$ trimer (Table VI) of PdAg/Pd(111) surface alloys are slightly lower than the corresponding adsorption energies on clean Pd(111) (Table IV), in spite of the slight upshift of the local *d*-band center shown in in Fig. 3 which would predict stronger adsorption. The physical reason for this discrepancy can only be speculated upon. Apparently, there is some longer-range interaction with the surrounding Ag atoms in the first layer that weakens the interaction with adsorbed CO. Similar, but vertical instead of lateral long-range effect have been observed for Pd/Au(111) [14] and Pt/Au(111) [58, 59] pseudomorphic overlayers. Tenney *et al.* show that in Ni-Au [51] and Pt-Au [52] clusters deposited on titania, Ni and Pt atoms can migrate, in each case, to the cluster surface in the presence of CO. If we compare with the PdAg surface alloy, this would indicate that palladium atoms will prefer to be on the topmost overlayer in order to adsorb CO molecules, implying larger adsorption energies when that layer is completely cover by palladium.

TABLE VI. CO adsorption energies (in eV) calculated using PBE/PAW for the PdAg/Pd(111) surface alloy considering Pd$_1$, Pd$_2$, Pd$_3$, and Pd$_4$ ensembles. Letters T, H, B denote top, hollow and bridge sites, respectively. Bold values denote the preferential adsorption sites in each case. CO coverage is 1/9.

		PBE/PAW		
	site	PdAg/Pd$_{4L}$	PdAg/Ag$_{1L}$/Pd$_{3L}$	PdAg/Ag$_{2L}$/Pd$_{2L}$
Pd$_1$	T	**−1.37**	**−1.14**	**−1.22**
Pd$_2$	B	**−1.64**	**−1.34**	**−1.41**
	T	−1.42	−1.05	−1.16
Pd$_3$	H-fcc	**−1.97**	−1.50	−1.65
	H-hcp	−1.90	**−1.52**	**−1.68**
	T	−1.46	−1.01	−1.14
Pd$_4$	H-fcc	**−1.97**	−1.48	−1.62
	H-hcp	−1.95	**−1.50**	**−1.67**
	T	−1.42	−1.05	−1.13

Underlying silver layers lead to smaller CO binding energies (up to $\sim$ 0.5 eV), as expected from the observed down-shift of the local *d*-band center plotted in Fig. 6. These findings are in agreement with experimental observations [53] of a reduced CO adsorption energy at top sites of a PdAg/Pd(111) surface alloy with a high Ag surface content so that the Pd monomers are surrounded by Ag atoms also in the second layer. Note, however, that the energy differences between hollow and top sites remain almost unchanged upon introducing Ag subsurface layers but the energy ordering between hollow-fcc and hollow-hcp sites becomes affected.

So far we have focused on the CO adsorption behaviour at low CO_{ad} coverages. At higher CO_{ad} coverages, CO adsorption may change drastically because of the additional effects caused by interactions between neighbouring CO_{ad} species. Experiments indeed suggested a re-accommodation of adsorbed CO molecules upon uptake of additional CO molecule(s) per Pd_2 or Pd_3 ensemble. [53] A similar effect was also shown by Wouda *et al.*, [42] for a PdAg bulk alloy surface. They observed that oxygen adsorption occurs only at palladium sites and migration of O atoms occurs stepping at the Pd sites. In that system, due to the high segregation of silver, the amount of palladium ensembles is very low, and they play an active role to allow the dissociation of O_2 molecules.

Table VII shows the calculated CO adsorption energies on Pd_2 and Pd_3 ensembles of the PdAg/Pd(111)$_{4L}$ surface alloy for different CO_{ad} coverages. For low CO_{ad} coverages, adsorption is favored at the bridge site of Pd_2 and at the hollow-fcc site of the Pd_3 and Pd_4 ensembles. An increase of CO_{ad} coverage indeed leads to a re-accommodation of the pre-adsorbed CO molecules above the Pd ensembles as suggested in the experimental study. [53] Since CO adsorption on silver sites is not favorable, CO is preferentially adsorbed at different top-sites of a palladium ensemble.

Compared to adsorption on the most stable sites of Pd_2 dimers or Pd_3 trimers, the adsorption energy of the two or three on top adsorbed CO is drastically reduced, by 0.33 eV (Pd_2 dimer) or even 0.68 eV (Pd_3 trimer) These changes, however, are mostly due to the change in adsorption site. The actual effect of the (repulsive) CO_{ad} - CO_{ad} interaction is better illustrated when comparing with CO adsorption at an on top site of the respective ensemble. In this case, the binding strength decreases only slightly due to the mutual repulsion of the CO molecules at the adjacent top sites.

The rather small change in binding strength with increasing CO_{ad} coverage compared to CO adsorption on Pd(111), where the adsorption energy is known to decay by about 0.5 eV in the range of high CO_{ad} coverages (see Table IV), is qualitatively understood by the lack of neighbouring CO_{ad} species outside the Pd_x ensemble. Although we do not find a significant outward tilt or lateral displacement in the adsorbed CO molecules at high coverages, this is obviously sufficient for a strongly reduced intermolecular repulsion. (Apparently, a bending of the CO molecules towards the inert Ag atoms is energetically not favorable.) It should be noted that the local CO_{ad} saturation coverage of $\Theta_{CO} = 1$ is higher than the saturation coverage obtained on Pd(111) ($\Theta_{CO,sat} = 0.75$ [94, 96]) Similarly high local coverages and rather small CO_{ad}–CO_{ad} repulsions were reported also for CO adsorption on PdAu/Pd(111) surface alloys by Ruff *et al.* [28] These authors calculated the net interaction for the case of two CO molecules adsorbed on Pd2 in the PdAu alloy to be $\sim$0.19 eV, which is rather similar to the value obtained in this study for adsorption at the PdAg surface alloy.

In the experiments, [53] for a Pd surface content of 25-39% in the PdAg/Pd(111) surface alloys, additional TPD peaks in CO desorption at 324-329 K were detected, at a lower temperature than those peaks attributed to desorption from the top sites of Pd monomers at very low Pd surface content. The peaks were associated with desorption of a second CO molecule adsorbed on a Pd_2 dimer (or the second and third molecule on a Pd_3 trimer). The scenario to understand this low desorption temperature and thus the low apparent binding energy is illustrated in Fig. 9. The most favorable adsorption site for a single CO molecule on a Pd dimer is the bridge site with an adsorption energy of -1.64 eV. The adsorption energy of a single CO molecule at the top site of a Pd_2 dimer is reduced to -1.42 eV, and if two CO molecules are adsorbed at both top sites, the mutual repulsion leads to an average adsorption energy of -1.31 eV.

However, both CO_{ad} molecules do not desorb simultaneously. Rather, one CO_{ad} molecule desorbs and leaves the other CO molecule initially alone at the other top site. If this CO_{ad} remained at the top site, the appropriate desorption energy in the absence of any additional desorption barrier would be 1.20 eV, which is lower than the desorption from an isolated Pd_1 top site. However, as

TABLE VII. CO adsorption energies (in eV) calculated using PBE/PAW, for the PdAg/Pd(111)$_{4L}$ surface alloy considering Pd_2, and Pd_3 ensembles and the effect of increasing CO coverage. Letters T, H, B denote top, hollow and bridge sites, respectively. Cases labeled with 2T and 3T denote CO adsorption occurring at two or three top-sites of the same ensemble.

			PBE/PAW	
	site	θ_{CO}	referred to Pd_n	referred to CO_{ad}/Pd_n
Pd_2	B	1/9	−1.64	–
	T	1/9	−1.42	0.22
	2T	2/9	−1.31	−1.20 (CO_{ad} at T)
	2T	2/9	−1.31	−0.98 (CO_{ad} at B)
Pd_3	H-fcc	1/9	−1.97	–
	T	1/9	−1.46	0.51
	2T	2/9	−1.35	−1.23 (CO_{ad} at T)
	2T	2/9	−1.35	−0.72 (CO_{ad} at H)
	3T	1/3	−1.29	−1.17 (CO_{ad} at 2T)

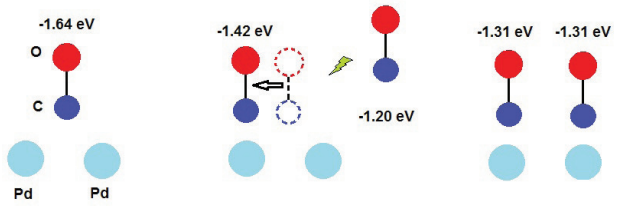

FIG. 9. Simplified illustration of CO adsorption on a Pd_2 ensemble under high CO exposure conditions. **Left:** Preferred adsorption of one CO molecule at the bridge site of Pd_2. **Center:** Energetics relevant for the additional adsorption of a CO molecule on a Pd_2 dimer. Repulsion from neighbor CO molecules shifts the first absorbed CO molecule away to one top site and reduces its adsorption energy. A second CO molecule will be adsorbed at the other top site. **Right:** Final stage showing simultaneous adsorption at the top sites, that leads to an averaging of both adsorption energies. (Pd: cyan, C: blue, O: red).

the CO molecule leaves the Pd_2 ensemble, the other CO_{ad} molecule will relocate from the on-top site to the more stable bridge site. The net energy loss of the remaining ensemble, which again in the absence of additional desorption barriers corresponds to the relevant desorption energy, is therefore only $2 \times 1.31 - 1.64 = 0.98\,\text{eV}$, which is significantly lower than desorption from an isolated Pd_1 top site. The mechanism is illustrated for the time-reverse process, the adsorption of two CO molecules on a Pd_2 dimer. These results confirm the experimental assignment of the desorption peaks.

V. CONCLUSIONS

The structure and local reactivity of PdAg/Pd(111) surface alloys were studied using periodic density functional theory calculations. As a probe of the local reactivity, CO adsorption energies were evaluated and compared to the results of a recent experimental study. [53] We find that the formation of one pseudomorphic Ag overlayer on Pd(111) is energetically most stable compared to the segregation of the bimetallic PdAg system into Pd(111) and Ag bulk, due to the strong Pd-Ag interaction. As far as the formation of PdAg/Pd(111) surface alloys at low Pd concentrations in the first layer is concerned, the formation of compact Pd structures is more stable than any random configuration. For PdAg surface alloys with approximately equal Pd and Ag concentrations, the replacement of the Pd subsurface layer by a Ag subsurface layer is energetically favorable, in agreement with the experimental observation of the interdiffusion between Ag film and Pd substrate at annealing temperatures above 500 K.

On Pd(111), CO prefers high-coordinated sites, i.e., three-fold hollow sites. The same is true for PdAg/Pd(111) surface alloys. Hence we find a strong ensemble effect. Once Pd_3 trimers are available in the surface alloys, they become the most favorable adsorption sites, followed by Pd_2 dimers (bridge site) and finally Pd_1 monomers (on top sites). In contrast, we only find a small ligand effect due to two opposing effects: Increasing the number of, e.g., Pd atoms in the surface alloys reduces the tensile strain which should increase the local reactivity, but it also increases the interaction with other Pd atoms which decreases the local reactivity. Both effects almost cancel each other for PdAg/Pd(111) surface alloys.

Replacing Pd in the subsurface layer by Ag surprisingly leads to weaker CO binding to small Pd ensembles in the surface alloy which is also reflected in a corresponding downshift of the local Pd *d*-band center. Upon higher exposure of CO to PdAg/Pd(111) surface alloys with small Pd ensembles (dimers, trimers), the small Pd ensembles can adsorb more than one CO molecule. When it occurs, the preferential absorption moves from hollow sites to top sites, but with smaller adsorption energies due to the mutual repulsion between the CO molecules. These results, as all other observed trends in the adsorption energies as a function of the composition of the PdAg/Pd(111) surface alloy, are consistent with previous experimental observations. [53] indicating the reliability of DFT calculations to reproduce and explain trends in the local reactivity of surface alloys.

ACKNOWLEDGMENTS

This work has been supported by the German Science Foundation (DFG) through the Research Unit 1376, contracts GR 1503/22-1 and BE 1201/18-1.

[1] J. H. Sinfelt, Surf. Sci. **500**, 923 (2002).
[2] V. Ponec, Applied Catalysis A: General **222**, 31 (2001).
[3] A. Groß, Top. Catal. **37**, 29 (2006).
[4] M. Del Popolo et al., Appl. Phys. Lett. **81**, 2635 (2002).
[5] A. Roudgar and A. Groß, Surf. Sci. **559**, L180 (2004).
[6] O. R. Inderwildi, S. J. Jenkins, and D. A. King, Surf. Sci. **601**, L103 (2007).
[7] H. Baltruschat and S. Ernst, ChemPhysChem **12**, 56 (2011).
[8] F. Illas et al., J. Phys. Chem. B **102**, 8017 (1998).
[9] A. Roudgar and A. Groß, Surf. Sci. **597**, 42 (2005).
[10] A. Bergbreiter, H. E. Hoster, S. Sakong, A. Groß, and R. J. Behm, Phys. Chem. Chem. Phys. **9**, 5127 (2007).
[11] F. Buatier de Mongeot, M. Scherer, B. Gleich,

E. Kopatzki, and R. J. Behm, Surf. Sci. **411**, 249 (1998).
[12] A. Schlapka, M. Lischka, A. Groß, U. Käsberger, and P. Jakob, Phys. Rev. Lett. **91**, 016101 (2003).
[13] F. Maroun, F. Ozanam, O. M. Magnussen, and R. J. Behm, Science **293**, 1811 (2001).
[14] A. Roudgar and A. Groß, J. Electroanal. Chem. **548**, 121 (2003).
[15] L. A. Kibler, A. M. El-Aziz, R. Hoyer, and D. M. Kolb, Ang. Chemie, Int. Ed. **44**, 2080 (2005).
[16] R. Ferrando, J. Jellinek, and R. L. Johnston, Chem. Rev. **108**, 845 (2008).
[17] J. Greeley and M. Mavrikakis, Nat. Mater. **3**, 810 (2004).
[18] V. Ponec and W. Sachtler, J. Catal. **24**, 250 (1972).
[19] J. Sinfelt, J. Carter, and D. Yates, J. Catal. **24**, 283 (1972).
[20] Y. Soma-Noto and W. Sachtler, J. Catal. **32**, 315 (1974).
[21] W. M. H. Sachtler, Catal. Rev. **14**, 193 (1976).
[22] J. Sachtler and G. Somorjai, J. Catal. **81**, 77 (1983).
[23] J. A. Rodriguez, Surf. Sci. Rep. **24**, 223 (1996).
[24] W. M. H. Sachtler, Faraday Discuss. Chem. Soc. **72**, 7 (1981).
[25] S. Sakong, C. Mosch, and A. Groß, Phys. Chem. Chem. Phys. **9**, 2216 (2007).
[26] M. Mavrikakis, B. Hammer, and J. K. Nørskov, Phys. Rev. Lett. **81**, 2819 (1998).
[27] E. Demirci, C. Carbogno, A. Groß, and A. Winkler, Phys. Rev. B **80**, 085421 (2009).
[28] M. Ruff, N. Takehiro, P. Liu, J. K. Nørskov, and R. J. Behm, ChemPhysChem **8**, 2068 (2007).
[29] J. G. Chen, C. A. Menning, and M. B. Zellner, Surf. Sci. Rep. **63**, 201 (2008).
[30] A. Groß, J. Phys.: Condens. Matter **21**, 084205 (2009).
[31] N. Mouaddib, K. R. Thampi, A. J. McEvoy, J. Kiwi, and M. Grätzel, Catal. Lett. **5**, 285 (1990).
[32] J. Shu, B. P. A. Grandjean, A. V. Neste, and S. Kaliaguine, Can. J. Chem. Eng. **69**, 1036 (1991).
[33] Y. Jin et al., J. Catal. **203**, 292 (2001).
[34] H. Zea et al., Appl. Catal. A **282**, 237 (2005).
[35] Q. Zhang, J. Li, X. Liu, and Q. Zhu, Appl. Catal. A **197**, 221 (2000).
[36] I. Coulthard and T. K. Sham, Phys. Rev. Lett. **77**, 4824 (1996).
[37] G. Slusser and N. Winograd, Surf. Sci. **84**, 211 (1979).
[38] S.-Y. Lu and Y.-Z. Lin, Thin Solid Films **376**, 67 (2000).
[39] C. G. Sonwane, J. Wilcox, and Y. H. Ma, J. Phys. Chem. B **110**, 24549 (2006).
[40] L. Semidey-Flecha and D. S. Sholl, J. Chem. Phys. **128**, 144701 (2008).
[41] Z. Jovanović, M. D. Francesco, S. Tosti, and A. Pozio, Int. J. Hydrogen Energy **36**, 7728 (2011).
[42] P. T. Wouda, M. Schmid, B. Niewenhuys, and P. Varga, Surf. Sci. **423**, L229 (1999).
[43] S. Crampin, J. Phys.: Condens. Matter **5**, L443 (1993).
[44] M. Ropo, K. Kokko, L. Vitos, and J. Kollár, Phys. Rev. B **71**, 045411 (2005).
[45] G. Battaglin et al., Nuclear Instruments and Methods in Physics Research Section B **191**, 392 (2002).
[46] A. Godinez-Garcia, J. F. Perez-Robles, H. V. Martinez-Tejada, and O. Solorza-Feria, Mater. Chem. Phys. **134**, 1013 (2012).
[47] Y. Han, M. Zhang, W. Li, and J. Zhang, Phys. Chem. Chem. Phys. **14**, 8683 (2012).
[48] O. Lechner, *Spectroscopic investigation of zeolite supported PdAg and PtAg bimetallic clusters*, PhD thesis, University of Stuttgart, Germany, 2012.
[49] B. Eisenhut, J. Stober, G. Rangelov, and T. Fauster, Phys. Rev. B **47**, 12980 (1993).
[50] R. Fischer, T. Fauster, and W. Steinmann, Phys. Rev. B **48**, 15496 (1993).
[51] S. A. Tenney et al., J. Phys. Chem. C **115**, 11112 (2011).
[52] S. A. Tenney et al., J. Phys. Chem. C **114**, 21652 (2010).
[53] Y. Ma, T. Diemant, J. Bansmann, and R. J. Behm, Phys. Chem. Chem. Phys. **13**, 10741 (2011).
[54] Y. Ma, J. Bansmann, T. Diemant, and R. Behm, Surf. Sci. **603**, 1046 (2009).
[55] A. K. Engstfeld, H. E. Hoster, and R. J. Behm, Phys. Chem. Chem. Phys. **14**, 10754 (2012).
[56] A. P. Farkas, T. Diemant, J. Bansmann, and R. J. Behm, ChemPhysChem **13**, 3516 (2012).
[57] P. Liu and J. K. Nørskov, Phys. Chem. Chem. Phys. **3**, 3814 (2001).
[58] Y. Gohda and A. Groß, Surf. Sci. **601**, 3702 (2007).
[59] Y. Gohda and A. Groß, J. Electroanal. Chem. **607**, 47 (2007).
[60] M. Lischka, C. Mosch, and A. Groß, Electrochim. Acta **52**, 2219 (2007).
[61] J. Greeley, J. K. Nørskov, L. A. Kibler, A. M. El-Aziz, and D. M. Kolb, ChemPhysChem **7**, 1032 (2006).
[62] L. A. Kibler, ChemPhysChem **7**, 985 (2006).
[63] M. E. Björketun et al., Phys. Rev. B **84**, 045407 (2011).
[64] P. Quaino, E. Santos, H. Wolfschmidt, M. A. Montero, and U. Stimming, Catal. Today **177**, 55 (2011).
[65] G. Kresse and J. Furthmüller, Phys. Rev. B **54**, 11169 (1996).
[66] J. P. Perdew, K. Burke, and M. Ernzerhof, Phys. Rev. Lett. **77**, 3865 (1996).
[67] B. Hammer, L. B. Hansen, and J. K. Nørskov, Phys. Rev. B **59**, 7413 (1999).
[68] P. E. Blöchl, Phys. Rev. B **50**, 17953 (1994).
[69] G. Kresse and D. Joubert, Phys. Rev. B **59**, 1758 (1999).
[70] G. Kresse and J. Furthmüller, Comp. Mat. Sci. **6**, 15 (1996).
[71] R. W. G. Wyckoff, *Crystal structures*, volume 1, Interscience Publishers, New York, 1963.
[72] W. Humphrey, A. Dalke, and K. Schulten, J. Mol. Graph. **14**, 33 (1996).
[73] V. Blum et al., Comput. Phys. Commun. **180**, 2175 (2009).
[74] N. E. Singh-Miller and N. Marzari, Phys. Rev. B. **80**, 235407 (2009).
[75] M. Methfessel, D. Hennig, and M. Scheffler, Phys. Rev. B **46**, 4816 (1992).
[76] L. Vitos, A. V. Ruban, H. L. Skriver, and J. Kollar, Surf. Sci. **411**, 186 (1998).
[77] J. L. Da Silva, C. Stampfl, and M. Scheffler, Surf. Sci. **600**, 703 (2006).
[78] M. Ropo, K. Kokko, and L. Vitos, Phys. Rev. B **77**, 195445 (2008).
[79] L. Z. Mezey and J. Giber, Japanese J. of Appl. Phys. **21**, 1569 (1982).
[80] W. Tyson and W. Miller, Surf. Sci. **62**, 267 (1977).
[81] J. P. Perdew et al., Phys. Rev. Lett. **100**, 136406 (2008).
[82] S. V. Barabash, V. Blum, S. Müller, and A. Zunger, Phys. Rev. B **74**, 035108 (2006).
[83] G. Rangelov, T. Fauster, U. Strüber, and J. Küppers, Surf. Sci. **331-333**, 948 (1995).
[84] B. Hammer and J. K. Nørskov, Surf. Sci. **343**, 211 (1995).
[85] B. Hammer, Top. Catal. **37**, 3 (2006).

[86] A. Groß, J. Comput. Theor. Nanosci. **5**, 894 (2008).
[87] S. Sakong and A. Groß, Surf. Sci. **525**, 107 (2003).
[88] S. Surnev et al., Surf. Sci. **470**, 171 (2000).
[89] T. Gießel et al., Surf. Sci. **406**, 90 (1998).
[90] P. Sautet, M. Rose, J. Dunphy, S. Behler, and M. Salmeron, Surf. Sci. **453**, 25 (2000).
[91] P. J. Feibelman et al., J. Phys. Chem B. **105**, 4018 (2001).
[92] I. Grinberg, Y. Yourdshahyan, and A. M. Rappe, J. Chem. Phys. **117**, 2264 (2002).
[93] R. A. Olsen, P. H. T. Philipsen, and E. J. Baerends, J. Chem. Phys. **119**, 4522 (2003).
[94] X. Guo and J. T. Yates, J. Chem. Phys. **90**, 6761 (1989).
[95] G. McElhiney, H. Papp, and J. Pritchard, Surf. Sci. **54**, 617 (1976).
[96] F. M. Hoffmann, Surf. Sci. Rep. **3**, 107 (1983).

Structure and local reactivity of PdAg/Pd(111) surface alloys

Luis A. Mancera,[1,*] R. Jürgen Behm,[2] and Axel Groß[1,†]

[1] *Institute of Theoretical Chemistry, University of Ulm, Albert-Einstein-Allee 11, D-89069 Ulm, Germany*

[2] *Institute of Surface Chemistry and Catalysis, University of Ulm, Albert-Einstein-Allee 47, D-89069 Ulm, Germany*

Table of contents entry

The adsorption of CO on PdAg/Pd(111) has been studied by periodic DFT calculations, confirming and explaining experimental results that the adsorption on the surface alloy is dominated by ensemble effects, whereas electronic ligand and strain effects effectively cancel each other.

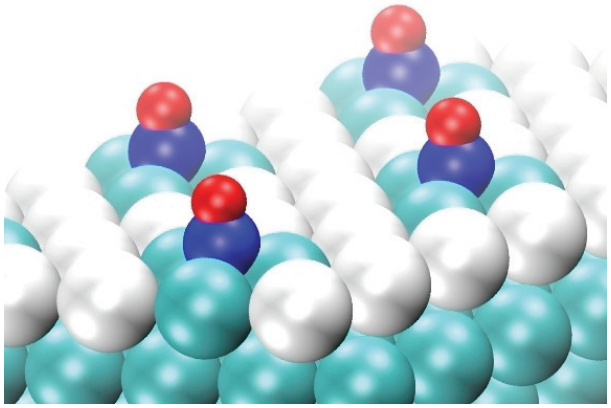

* luis.mancera@uni-ulm.de

† axel.gross@uni-ulm.de